The APPEA Journal 2021, **61**, 253–270
https://doi.org/10.1071/AJ20038

Peer reviewed paper

Petrophysical and geochemical interpretations of well logs from the pre-Carboniferous succession in Barnicarndy 1, Canning Basin, Western Australia

Liuqi Wang[A,D], *Dianne S. Edwards*[A], *Adam Bailey*[A], *Lidena K. Carr*[A], *Chris J. Boreham*[A], *Emmanuelle Grosjean*[A], *Leon Normore*[B], *Jade Anderson*[A], *Amber J. M. Jarrett*[A], *Susannah MacFarlane*[A], *Chris Southby*[A], *Chris Carson*[A], *Kamal Khider*[A], *Paul Henson*[A], *Peter Haines*[B] and *Mike Walker*[C]

[A]Geoscience Australia, GPO Box 378, Canberra, ACT 2601, Australia.
[B]Geological Survey of Western Australia, Locked Bag 100, East Perth, WA 6892, Australia.
[C]Walker Petrophysics Pty Ltd, Wyss Lane, North Lake, WA 6163, Australia.
[D]Corresponding author. Email: liuqi.wang@ga.gov.au

Abstract. Barnicarndy 1 is a stratigraphic well drilled in the southern part of the Canning Basin's Barnicarndy Graben under Geoscience Australia's Exploring for the Future program in collaboration with the Geological Survey of Western Australia to provide stratigraphic data for this poorly understood tectonic component. The well intersects a thin Cenozoic section, Permian–Carboniferous fluvial clastics and glacial diamictites and a thick pre-Carboniferous succession (855–2585 mRT) unconformably overlying Neoproterozoic metasedimentary rocks. Three informal siliciclastic intervals were defined based on core lithology, well logs, chemical and mineral compositions: the Upper Sandstone (855–1348.1 mRT), Middle Interval (1348.1–2443.4 mRT) and Lower Sandstone (2443.4–2585 mRT). The Middle Interval was further divided into six internal zones. Both conventional methods and artificial neural network technology were applied to well logs to interpret petrophysical and elastic properties, total organic carbon (TOC) content, pyrolysis products from the cracking of organic matter (S2) and mineral compositions. Average sandstone porosity and reservoir permeability are 17.9% and 464.5 mD in the Upper Sandstone and 6.75% and 10 mD in the Lower Sandstone. The Middle Interval claystone has an average porosity and permeability of 4.17% and 0.006 mD, and average TOC content and S2 value of 0.17 wt% and 0.047 mg HC/g rock, with maximum values of 0.66 wt% and 0.46 mg HC/g rock, respectively. Correlations of mineral compositions and petrophysical, geomechanical and organic geochemical properties of the Middle Interval have been conducted and demonstrate that these sediments are organically lean and lie within the oil and gas window.

Keywords: Canning Basin, elastic property, fluid inclusions, geochemical interpretation, Geological Survey of Western Australia, Geoscience Australia, hydrocarbon potential, mineral composition, neural network, organic and inorganic chemical composition, permeability, petrophysical interpretation, Pilbara, porosity, pre-Carboniferous, Barnicarndy 1, well log.

Received 17 December 2020, accepted 21 January 2021, published online 2 July 2021

Introduction

The Canning Basin is an intracratonic basin in Western Australia and occupies about 640 000 km^2, of which 530 000 km^2 are onshore. It has a maximum sediment thickness of over 15 000 m, from Early Ordovician to Early Cretaceous, in the two main NW-trending depocentres. The basin was initiated in the early Paleozoic as a NW-oriented intracratonic rift, and was later influenced by mid-Devonian–Carboniferous extension, mid-Carboniferous shortening and early Permian thermal sag (Kennard *et al.* 1994; Zhan and Mory 2013).

The Barnicarndy Graben (previously Waukarlycarly Embayment) lies in the eastern part of the Pilbara Mining District within the Shire of East Pilbara (Fig. 1) (Bagas *et al.* 2009; Alavi 2013). As part of Geoscience Australia's (GA) Exploring for the Future (EFTF) program, Barnicarndy 1 (previously Waukarlycarly 1) was drilled as a stratigraphic well at the southern part of the Barnicarndy Graben in the southwest Canning Basin in collaboration

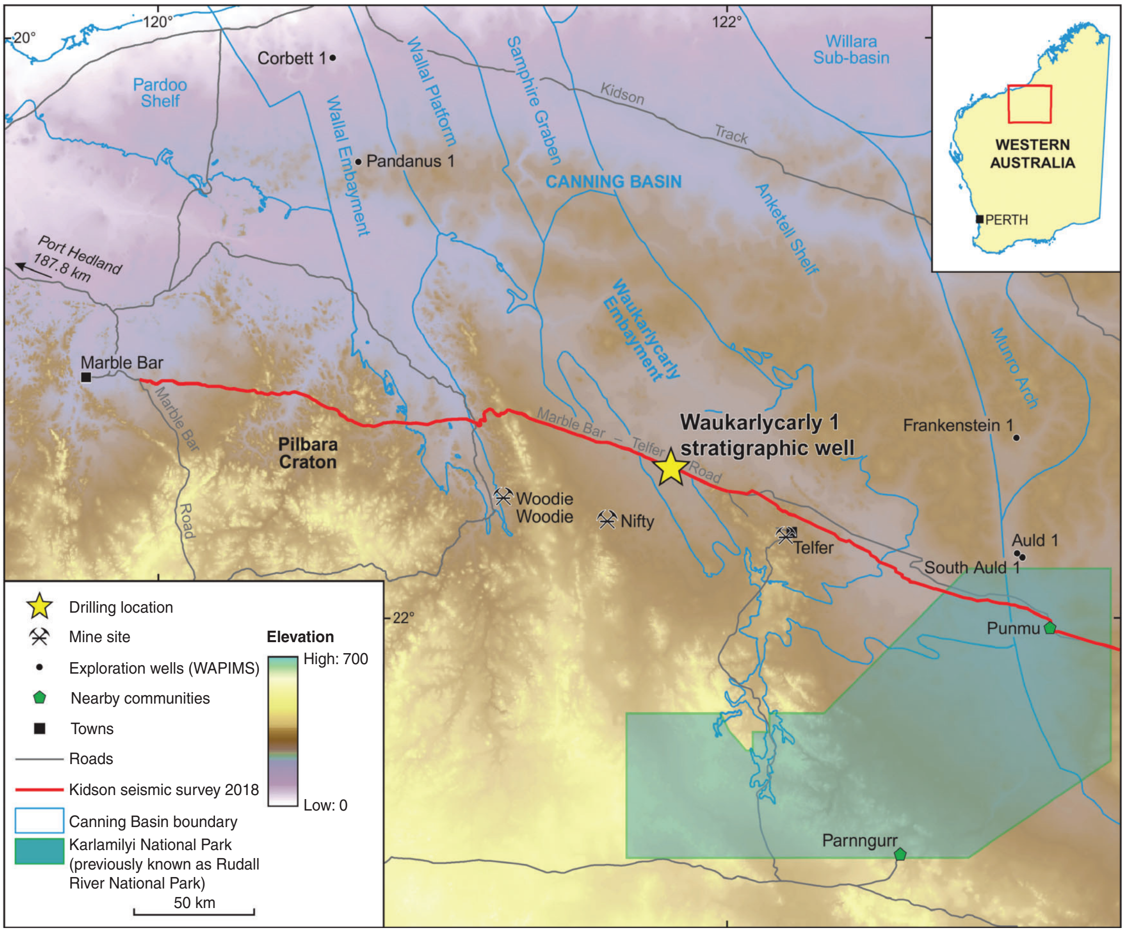

Fig. 1. Location of the Barnicarndy 1 well alongside the Kidson seismic line (18GA-KB1, red line) in the Barnicarndy Graben of the southwest Canning Basin (Normore and Rapaic 2020).

with the Geological Survey of Western Australia (GSWA). The wellsite is about 214 km east of Marble Bar and 51 km W-NW of the Telfer gold mine (Normore and Rapaic 2020; Normore and Zhan 2020) (Fig. 1). The drilling was a follow-up project to the 872 km Kidson seismic survey (18GA–KB1) to provide stratigraphic data for a poorly understood tectonic component of the southern Canning Basin (Carr *et al.* 2020).

Barnicarndy 1 was drilled to a total depth of 2680.53 mRT, penetrating a thin Cenozoic succession overlying Permian–Carboniferous fluvial clastics and glacial diamictites (Grant Group, Backhouse 2020; Normore *et al.* 2021 in preparation). Below the unconformity at the base of the Grant Group, a thick (1730 m) succession of pre-Carboniferous clastic rocks is present. Drilling was terminated in low-grade Neoproterozoic metasediments (Carr *et al.* 2020). Besides the cuttings collected from the surface to 580 mRT, three stages of continuous coring were carried out to total depth. Both core and cuttings were analysed using the GSWA HyLogger-3 (GSWA 2020*a*, 2020*b*). A series of laboratory tests were conducted on radioactive, petrophysical, geomechanical, fluid inclusion, organic and inorganic geochemical properties organised by GSWA and GA (FIT 2020; Forbes *et al.* 2020; Grosjean *et al.* 2020; Jarrett *et al.* 2020; Ranasinghe and Crosdale 2020; Core Lab 2020*a*, 2020*b*; Edwards *et al.* 2021). Well logging data were acquired by Wireline Services Group (WSG) to a depth of 1602.8 mRT and by Weatherford Logging to a depth of 2679.29 mRT. Walker Petrophysics Pty Ltd (2020) collected the raw log data and provided data pre-processing and interpretation on the shale fraction, total porosity, dynamic elastic properties, formation water resistivity and mineral compositions with five mineral components. Geothermal gradient was assessed as 28 °C/km at Barnicarndy 1, while the surface temperature was assumed to be 25 °C (Walker Petrophysics Pty Ltd 2020). Well data and the basic well completion report are available through the Western Australian Petroleum and Geothermal Information Management System (WAPIMS) provided by the Government of Western Australia (GSWA 2020*c*; Normore and Rapaic 2020).

In this study, the conventional petrophysical interpretation focuses on the effective porosity, water saturation and elastic properties. Permeability, organic geochemical properties and mineral compositions were interpreted using artificial neural network (ANN) technology. All of the petrophysical interpretations were conducted utilising Schlumberger's Techlog platform (Schlumberger 1991; Wang *et al.* 2021). The interpretations were focused on the depth range of 855–2585 mRT, which is beneath the base of the Grant Group and above the Neoproterozoic basement.

Petrophysical interpretation

Definition of internal intervals

Within the depth range of 855–2585 mRT (Fig. 2), two orders of lithological intervals were defined on the basis of vertical distribution patterns from chemostatigraphic packages (Forbes *et al.* 2020); well logs (Wang *et al.* 2021), mineral assemblages from HyLogger thermal infrared (TIR) (GSWA 2020*b*); responses of hydrocarbon, acetic acid and total response from fluid inclusion stratigraphy (FIS) testing results (FIT 2020); chemical compositions from inductively coupled plasma (ICP) testing results (Forbes *et al.* 2020); and mineral assemblages from X-ray diffraction (XRD) and scanning electron microscopy (SEM) analysis results (Core Lab 2020*b*; Edwards *et al.* 2021). The ICP tests included both the optical emission spectrometry (ICP-OES) and mass spectrometry (ICP-MS) (Forbes *et al.* 2020). Laboratory testing results, core lithology and well logs demonstrate the lithofacies variations and good correlations with each other.

At the first order (Zone_EFTFIntS), three major zones are defined: an Upper Sandstone, a Middle Interval and a Lower Sandstone (Fig. 2 and Table 1). From oldest to youngest, the Lower Sandstone mainly contains greyish orange to dark red/brown, fine to very fine sandstone with greyish orange, very fine to very coarse sandstone beds. As well as clastic rocks, thin pale green to dark red/brown ash beds or tuffaceous matter are also observed in the core. The Lower Sandstone corresponds with Package 2 of Forbes *et al.* (2020), which is defined based on chemostratigraphy and contains fluid inclusions with high hydrocarbon peaks (FIT 2020). The Middle Interval is dominated by thick claystone with a small portion of siltstone/sandstone and minor dolomite/limestone beds. The claystones are variably dolomitic, calcareous and silty. This zone corresponds with Packages 3–6 of Forbes *et al.* (2020) and is identified as an Ordovician succession by Normore *et al.* (2021). The lithofacies variations are identified on well logs, in the mineral components from HyLogger TIR, and from chemical and mineral compositions (Fig. 2). The Upper Sandstone is characterised by quartz sandstone with minor claystone beds, and its lower part corresponds to Package 7 (P_7, Forbes *et al.* 2020). The Upper Sandstone is present below the unconformity at the base of Grant Group and is regarded as a lower Paleozoic succession, although the age of this zone is undetermined due to a lack of biostratigraphic and geochronological data (Normore *et al.* 2021).

The first order Middle Interval is further divided into six second order zones (Zone_EFTFInt), as shown in Fig. 2. These are defined on variations in lithofacies and mineral assemblages and are, from oldest to youngest, M_1 to M_6 (Fig. 2). M_1 contains mainly dark grey claystone with evidence for fossilised burrows. M_2 contains various lithofacies types, including fine to very fine sandstone, siltstone and claystone, and claystone beds that are slightly to moderately dolomitic and silty. M_1 and M_2 occur over a similar depth ranges as Package 3 and 4 of Forbes *et al.* (2020). M_3 consists of dark grey to greyish black, slightly to moderately calcareous claystone with thin beds of grey limestone. Fossil fragments are observed in the argillaceous limestone beds. M_4 and M_5 are composed of dark grey to greyish black, variably calcareous claystone with thin beds of limestone, although M_5 is less calcareous than M_4. Fossilised burrows with slightly calcareous silts and very fine quartz fillings are observed in M_4. M_6 contains mainly claystone and siltstone beds, including brownish grey bioturbated siltstone and fine to very fine sandstone beds. The claystone is locally highly bioturbated, silty, slightly dolomitic and slightly to moderately calcareous. M_3 to M_5 are within Package 5, and M_6 corresponds to Package 6 of Forbes *et al.* (2020).

Effective porosity

Logged bulk density (RHOB, g/cm^3) was plotted against neutron porosity (NPHI, m^3/m^3) and these data are presented in Fig. 3. Data points from the Upper and Lower sandstones are mainly distributed along the sandstone polyline, whereas data from the Middle Interval are scattered across all three polylines. This implies that most claystone and siltstone/sandstone are likely to be either calcareous or dolomitic. These data provide the basis for an interpretation of effective porosity (Schlumberger 1991; Wang *et al.* 2021). The resultant interpreted effective porosity (POR and PHIE_ND) is presented alongside the laboratory measured effective porosity (Jarrett *et al.* 2020; Core Lab 2020*a*) in Fig. 4. A strong correlation is observed between the interpreted porosity and the laboratory measured porosity ($R^2 = 0.844$), implying good agreement between these datasets. Table 2 lists the averages of interval effective porosity (PHIE_ND) and claystone porosity (PHIE_NDsh).

The average effective porosity of sandstones (shale fraction from neutron-density crossplot (VSHND) < 0.5) in the Upper Sandstone, Middle Interval and Lower Sandstone are 17.9%, 5.7% and 6.75%, respectively. The average reservoir porosities (VSHND < 0.5 and PHIE_ND > 0.1) of the Upper Sandstone and Lower Sandstone are 18% and 12.7%, respectively, and the average porosity of claystone (VSHND > 0.5) is 4.17% in the Middle Interval. The average claystone porosity in various internal zones of the Middle Interval ranges from 2.2% to 6%. The ratios of reservoir/gross thickness in the Upper Sandstone and Lower Sandstone are 0.991 and 0.243, respectively.

Water saturation

In the FIS results (Fig. 4), sulfur species, including carbon disulfide plus hydrocarbons (S_2 + HCs), hydrogen sulfide (H_2S) and the ratio of hydrogen sulfide over the sum of hydrogen sulfide and methane ($H_2S/H_2S + CH_4$), are sporadically present in the Upper Sandstone, at 2447.4 mRT and over the depth range of 2550.3–2580.3 mRT. The presence of sulfur species is generally associated with water-bearing, porous reservoir rocks and the water saturation in the Upper Sandstone is 1.0 (fraction). In this study, effective water saturation interpretation was conducted in the Middle Interval and Lower Sandstone. The Simandoux equation was used to compute effective water saturation (Schlumberger 1991; Wang *et al.* 2021) using the formation water resistivity of 0.03 ohmm, tortuosity factor of 1.0, cementation exponent of 2.4 and saturation exponent of 2.0 from Pickett plotting (Walker Petrophysics Pty Ltd 2020). Water saturation was less than 1.0 (fraction) with the average of 0.97 (fraction) in the low porosity sandstone/siltstone beds in M_2 and equal to 1.0 (fraction) in other zones (Column 8, Fig. 4).

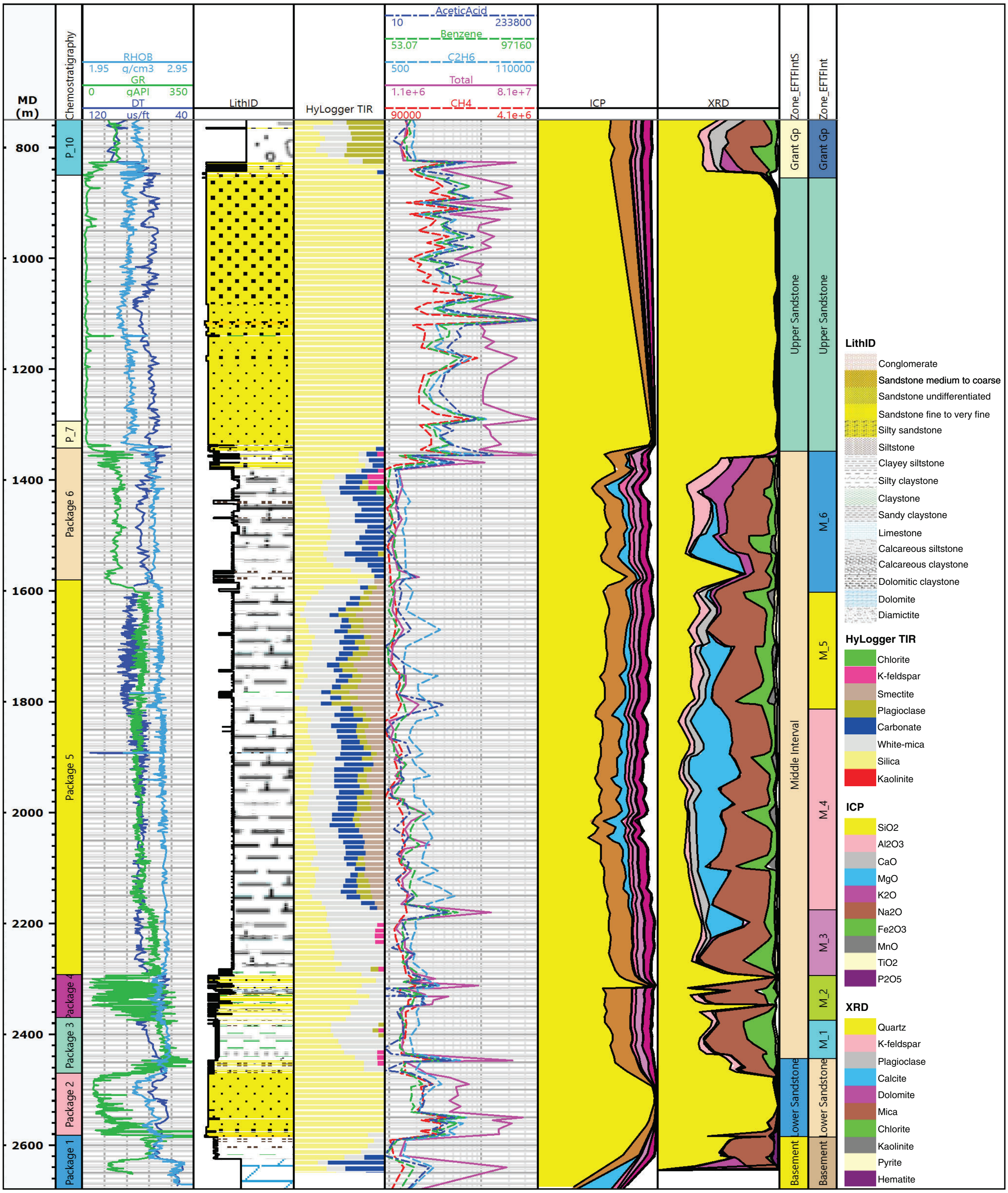

Fig. 2. Definition of internal zones based on lithological sequences, well logs, chemostratigraphy and mineral assemblages in Barnicarndy 1. Column 1: measured depth (MD); Column 2: chemostratigraphic packages; Column 3: gamma ray (GR), compressional slowness (DT) and bulk density (RHOB); Column 4: lithological descriptions of cores (LithID); Column 5: HyLogger thermal infrared results (TIR); Column 6: responses of methane (CH_4), ethane (C_2H_6), benzene, acetic acid and total from fluid inclusion results; Column 7: Inductively coupled plasma (ICP) testing results; Column 8: X-ray diffraction (XRD) results; Columns 9–10: two orders of lithological zones (Table 1).

Table 1. Lithological zones in the pre-Carboniferous succession in Barnicarndy 1

First order interval	Second order interval	Top depth (mRT)	Bottom depth (mRT)
Grant Group	Grant Group	96	855
Upper Sandstone	Upper Sandstone	855	1348.1
Middle Interval	M_6	1348.1	1602.6
	M_5	1602.6	1813.1
	M_4	1813.1	2175.7
	M_3	2175.7	2293.7
	M_2	2293.7	2374.7
	M_1	2374.7	2443.4
Lower Sandstone	Lower Sandstone	2443.4	2585
Basement	Basement	2585	2680

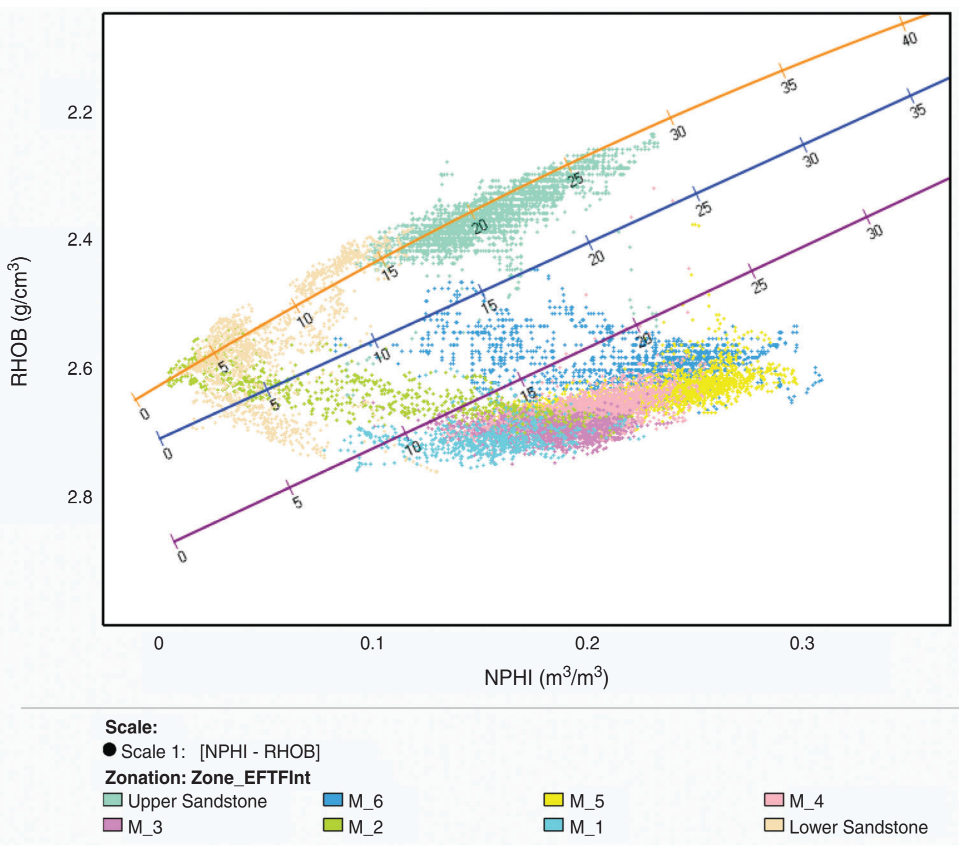

Fig. 3. Crossplot of bulk density (RHOB, g/cm^3) and neutron porosity (NPHI, m^3/m^3) from Weatherford logs in Barnicarndy 1. The polylines are from Weatherford compact neutron porosity-density chart (CM 6–10 compact log, Weatherford 2007), including sandstone polyline (orange), limestone polyline (blue) and dolomite polyline (purple).

Elastic property

Three potential reservoir/seal pairs from Barnicarndy 1 core were selected for measuring the static elastic properties in the laboratory, providing the averages of Poisson's ratio and Young's modulus as 0.1133 (fraction) and 13.3 GPa, respectively (Jarrett *et al.* 2020). Dynamic elastic properties, including Poisson's ratio (fraction) and Young's modulus (GPa), were calculated from bulk density (RHOB, g/cm^3), compressional and shear wave slowness (DT and DTSX, μs/ft) (Fig. 4) (Schlumberger 1991; Wang *et al.* 2021). These data,

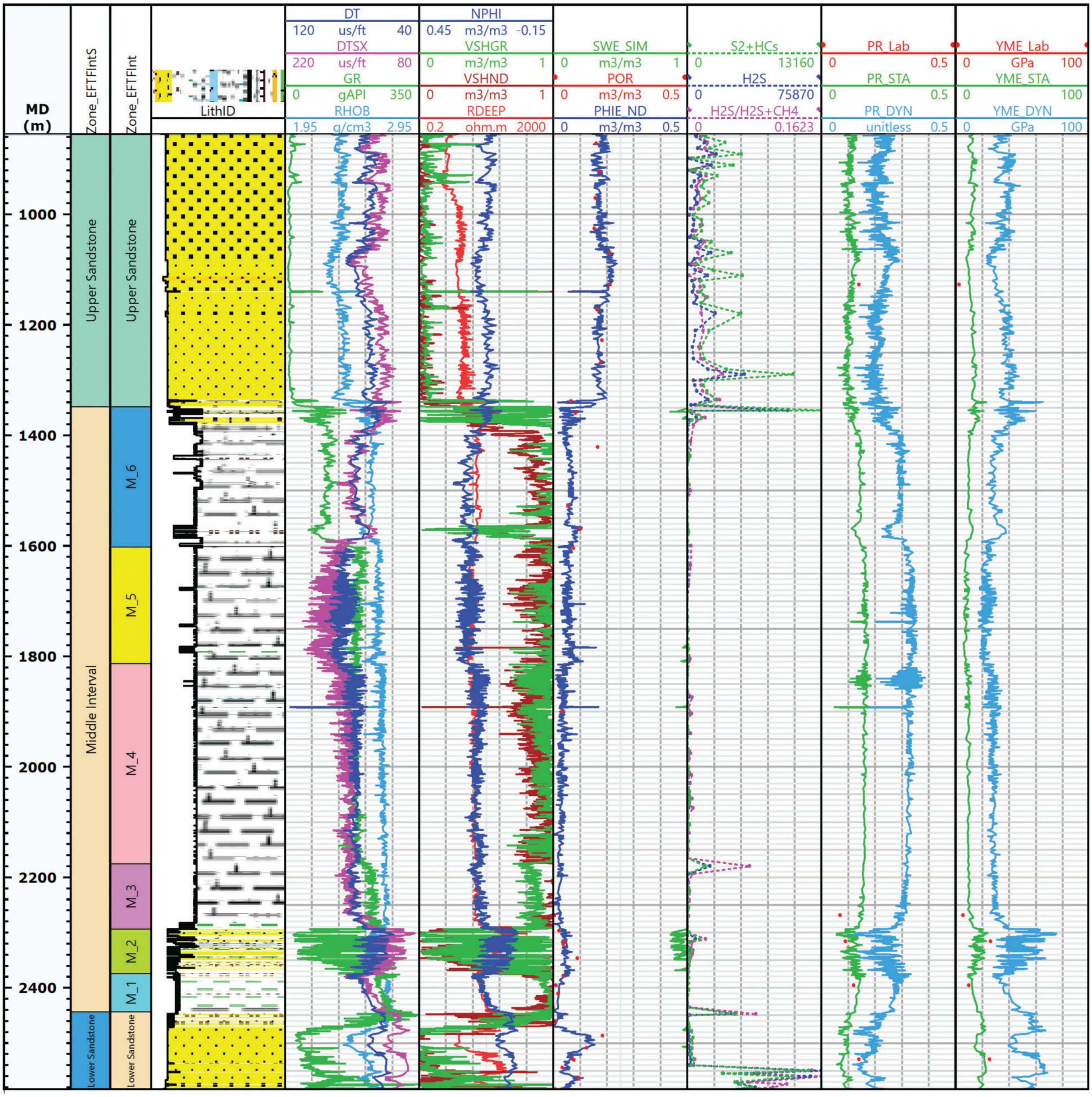

Fig. 4. Well logs and interpretation results of porosity, water saturation and elastic properties in Barnicarndy 1. Column 1: measured depth (MD); Columns 2–3: two orders of intervals (Zone_EFTFIntS and Zone_EFTFInt); Column 4: lithological descriptions of cores (LithID, same legend as in Fig. 2); Column 5: gamma ray (GR), compressional and shear slowness (DT and DTSX) and bulk density (RHOB); Column 6: limestone neutron porosity (NPHI), deep resistivity (RDEEP) and shale fractions from gamma ray and neutron-density crossplot (VSHGR and VSHND); Column 7: laboratory measured and interpreted porosity (POR and PHIE_ND) and interpreted water saturation (SWE_SIM); Column 8: carbon disulfide plus hydrocarbons ($S_2 + HCs$), hydrogen sulfide (H_2S) and the ratio of hydrogen sulfide over the sum of hydrogen sulfide and methane ($H_2S/H_2S + CH_4$); Column 9: dynamic, laboratory measured and converted static Poisson's ratio (PR_Lab, PR_DYN and PR_STA); Column 10: dynamic, laboratory measured and converted static Young's modulus (YME_Lab, YME_DYN and YME_STA).

when compared, provided a static/dynamic ratio of 0.4929 for Poisson's ratio and 0.3475 for Young's modulus. These ratios where used to convert calculated dynamic elastic properties to interpreted static properties, providing a continuous static curve for Poisson's ratio and Young's modulus (Fig. 4). Average values for the interpreted elastic properties in sandstones and claystones are provided in Table 3.

Laboratory measured, dynamic and converted static Poisson's ratio (PR_Lab, PR_DYN and PR_STA, fraction) are presented in Column 9 (Fig. 4). Laboratory measured, dynamic

Table 2. Averages of interval effective porosity (PHIE_ND) and claystone porosity (PHIE_NDsh) in the pre-Carboniferous succession in Barnicarndy 1

Zones	PHIE_ND (fraction)	PHIE_NDsh (fraction)
Upper Sandstone	0.179	0.066
M_6	0.063	0.060
M_5	0.056	0.055
M_4	0.032	0.032
M_3	0.023	0.022
M_2	0.044	0.046
M_1	0.025	0.025
Middle Interval	0.043	0.042
Lower Sandstone	0.067	0.005

Table 3. Averages of the interpreted static Poisson's ratio and Young's modulus in Barnicarndy 1

Rock type	Interval	Poisson's ratio (fraction)	Young's modulus (GPa)
Sandstone	Upper Sandstone	0.107	12.33
	Middle Interval	0.113	16.42
	Lower Sandstone	0.091	18.99
Claystone	Middle Interval	0.154	9.81

and converted static Young's modulus (YME_Lab, YME_DYN and YME_STA, GPa) are shown in Column 10 (Fig. 4).

Petrophysical interpretation using artificial neural network technology

Artificial neural network technology

ANN has been used to solve a wide variety of tasks (Hect-Nielsen 1990; Kalogirou 2000). In the petroleum domain, ANN has been applied in estimating hard data, such as laboratory measurements, from secondary (or soft) data, like seismic, well logs and conceptual geological data (Wong *et al.* 1995; Huang *et al.* 2001; Ouadfeul and Aliouane 2015). An example of a popular architecture of the three-layer perceptron in the Techlog platform (Wang *et al.* 2021) is provided in Fig. 5, including input, hidden and output layers. In this study, the input parameters include a series of selected well logs and one single output parameter.

The input of each neuron in hidden and output layers is a linear combination of neuron outputs in the former layer. By comparing to targets (laboratory measurements), the root mean square error (RMSE) can be written as:

$$RMSE = \sqrt{\frac{\sum (d_o - x_o)^2}{N}} \tag{1}$$

Where $(d_o - x_o)$ denotes the difference between the modelled output and input target and N is the number of traning patterns.

The error backpropagation technique was applied to optimise the weights during the neural net learning process (Hopfield 1985; Wong *et al.* 1995; Wang *et al.* 2021).

To avoid overlearning or overfitting, a validation patterns set was used to define the stopping epoch or cycle. The optimal stopping point or cycle is determined when the learning error of the training set stops decreasing significantly and the validation error reaches the lowest point. The neural network training with validation set may not learn all underlying relationships between input and output parameters since not all data is involved. Training with all training patterns are applied, particularly when there are not many training patterns. The stopping cycle is determined where error stops decreasing significantly. Generally, error tolerance and interactive interpretation need to be set by comparing the approximations with training targets on error changes, lithofacies variations, etc. (Wong *et al.* 1995).

Geochemical property interpretation

Total organic carbon (TOC) content indicates the richness of organic matter in sedimentary rocks. The TOC content can be correlated with conventional well log data, such as radioactive logs, porosity logs and resistivity logs (Schmoker 1981; Schmoker and Hester 1983; Passey *et al.* 1990; Herron 1991; Passey *et al.* 2010; Yan *et al.* 2014). However, those methods are based on empirical, linear and simple non-linear regressions and largely rely on the quality of log data. The relationships between TOC content and well logs can be complex and non-linear in different sedimentary basins (Wong *et al.* 1995; Ouadfeul and Aliouane 2015). The ANN learning was employed to learn these relationships and approximate TOC content from well logs in this study.

In total, 199 samples from Barnicarndy 1 were analysed on a Rock-Eval 6 instrument (Grosjean *et al.* 2020), which provided TOC content (wt %) and pyrolysis products from the cracking of organic matter (S2, mg HC/g rock: Behar *et al.* 2001). Due to the existence of pyrite, hematite, tuffaceous matter (ash beds) and uncertainties in well log data, it is difficult to estimate TOC content directly from gamma ray, density and porosity with resistivity logs. ANN technology was then used for geochemical property interpretation.

Training patterns for the 199 samples were constructed with one output parameter (TOC or S2) and five input parameters, including bulk density (RHOB, g/cm^3), compressional wave slowness (DT, μs/ft), gamma ray (GR, gAPI), limestone neutron porosity (NPHI, m^3/m^3) and deep resistivity (RDEEP, Ω m). For the validation purpose, randomly selected 170 training patterns were set as training patterns, while the remaining 29 patterns were set as validation patterns.

Laboratory measured and neural network approximations of TOC content (wt %) and S2 (mg HC/g rock) are presented in Fig. 6, Columns 7 and 8, respectively. The correlation coefficients (R) between the neural network estimated and laboratory measured TOC content and S2 are 0.8746 and 0.8367, respectively. Table 4 lists the averaged and maximum neural network interpreted TOC content (TOCsh and TOCshmax, wt %) and S2 of claystone (S2sh and S2shmax, mg HC/g rock) in different intervals. The average TOC content and S2 are 0.17 wt% and 0.047 mg HC/g rock in the Middle Interval (Table 4).

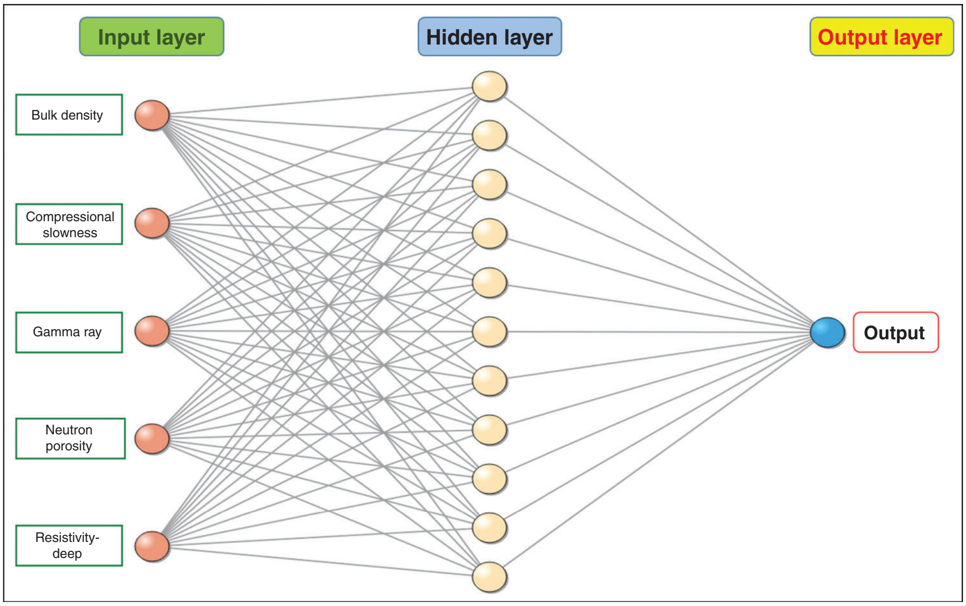

Fig. 5. Three-layer neural network architecture with multiple inputs and one output.

Permeability interpretation

In total, 38 permeability testing results (Jarrett *et al.* 2020; Core Lab 2020*a*) were used to construct 38 neural network training patterns, which had six input parameters, including bulk density (RHOB, g/cm^3), compressional wave slowness (DT, µs/ft), gamma ray (GR, gAPI), limestone neutron porosity (NPHI, m^3/m^3), deep resistivity (RDEEP, Ω m) and effective porosity (PHIE_ND, m^3/m^3) as well as one output parameter, permeability, for neural network training (Wong *et al.* 1995; Wang *et al.* 2021). Column 9 in Fig. 6 presents the laboratory measured, neural network estimated permeability and its smoothed result.

Table 5 lists the correlation coefficients (R) between the neural network estimated and laboratory measured permeability in Barnicarndy 1. The correlation coefficient in the high-permeability sandstone unit is higher than that from the low-permeability Middle Interval (Table 5), which shows difficulty in approximating permeability from well logs for claystone.

Table 6 presents the geometrical mean and maximum permeability of sandstone (VSHND < 0.5) of three major intervals and claystone in the Middle Interval. The geometric mean claystone permeability of different internal zones ranges from 0.002 to 0.122 mD.

Mineral composition interpretation

XRD tests were conducted on 101 samples from Barnicarndy 1, including 47 rotary sidewall core samples tested in Core Lab together with SEM analysis (Core Lab 2020*b*) and 54 core samples tested by Bureau Veritas (Edwards *et al.* 2021). The test results from Core Lab (2020*b*) include the weight percentages of quartz, anhydrite, potassium-feldspar (K-feldspar), plagioclase, calcite, dolomite/Fe-dolomite, hematite, pyrite, siderite, fluorapatite, sylvite, halite, TotalClay, illite/smectite, chlorite/smectite, illite and mica (includes biotite), kaolinite, chlorite, and percentages of smectite in illite/smectite and chlorite/smectite mixtures. The major mineral compositions include quartz, feldspar, carbonate, clay minerals, pyrite and hematite. In the Bureau Veritas data, the quantitative XRD testing using the X'Pert HighScore Plus search/match software provided the weight percentages of various mineral groups (Edwards *et al.* 2021), including chlorite, mica, kaolinite-serpentine, K-feldspar, plagioclase, hematite, pyrite, calcite and dolomite groups. The chlorite group includes chlorite, smectite, aerinite and vermiculite, and the mica group includes biotite, muscovite and illite. After a brief reorganisation, testing results from both sources show that there are mainly 10 types of mineral groups presented in the Barnicarndy 1 samples, including quartz, K-feldspar, plagioclase, calcite, dolomite, mica, chlorite, kaolinite, pyrite and hematite. The simplified assemblage includes quartz, feldspar (K-feldspar and plagioclase included), carbonate (calcite and dolomite included), TotalClay (mica, chlorite and kaolinite included), pyrite and hematite.

A linear system of equations has traditionally been used to estimate mineral compositions (Schlumberger 1991; Walker Petrophysics 2020), which offers a coarse guide to understand rock compositions. However, the linear system solvers require a set of good quality log curves and not too many minerals to solve, otherwise the problem would be mathematically undetermined. Besides the uncertainties in well logs, due to the complexity on mineral compositions, particularly in the Middle Interval, it is difficult to describe the mineral assemblage using conventional multi-mineral interpretations by solving a set of linear equations.

Neural network technology provides a different way to approximate mineral compositions from well logs by learning distribution patterns of both input and output parameters, which are related to the interior linear or non-linear relationships. In this study, the input parameters included gamma ray (GR, gAPI), bulk

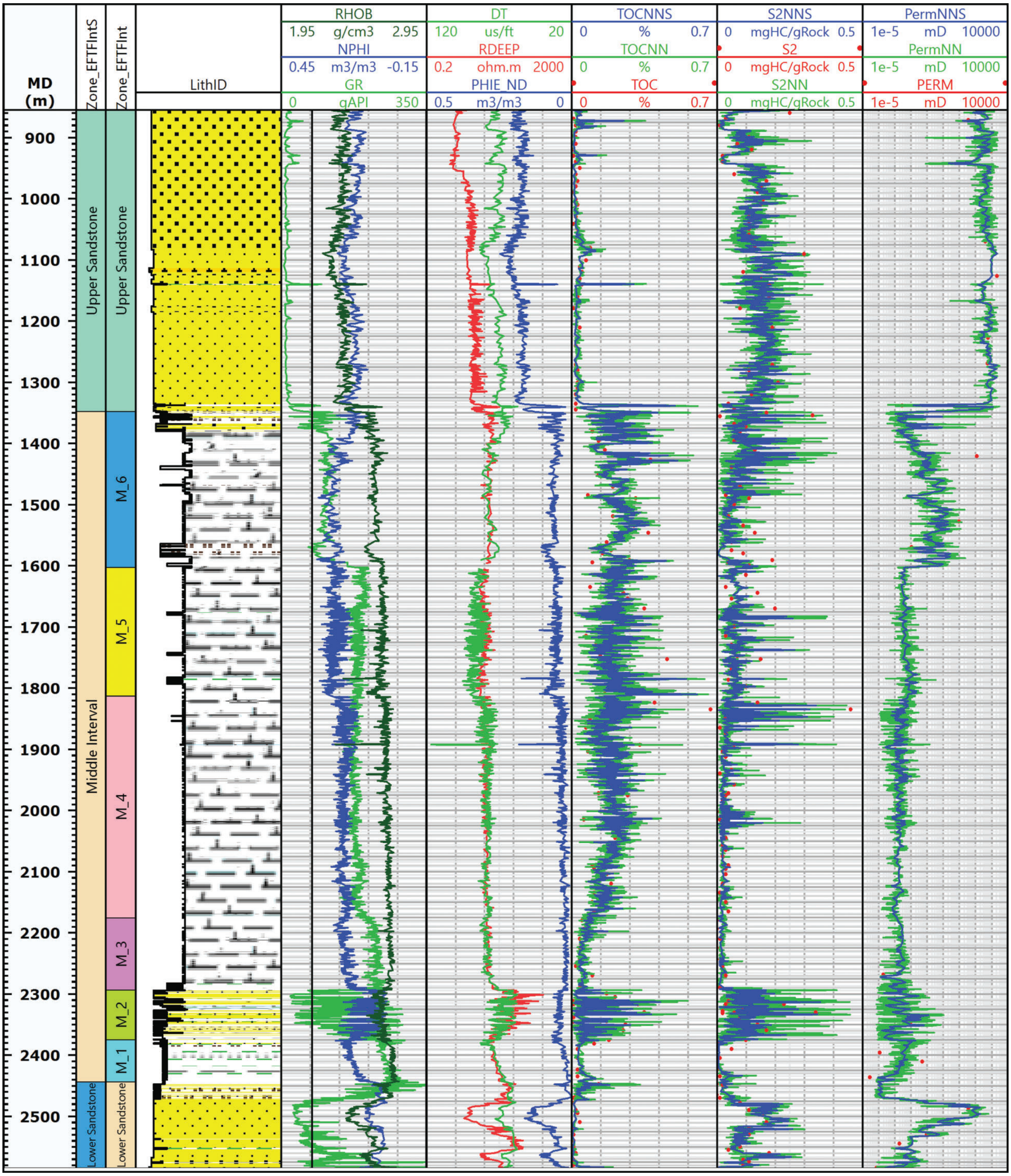

Fig. 6. Neural network interpretation results of TOC content, S2 and permeability. Column 1: measured depth (MD); Columns 2–3: two orders of zones (Zone_EFTFIntS and Zone_EFTFInt); Column 4: lithological descriptions of cores (LithID); Column 5: gamma ray (GR), limestone neutron porosity (NPHI) and bulk density (RHOB); Column 6: compressional slowness (DT), deep resistivity (RDEEP) and interpreted effective porosity (PHIE_ND); Column 7: laboratory measured, interpreted TOC content (TOC and TOCNN) and its smoothed result (TOCNNS); Column 8: laboratory measured, interpreted S2 (S2 and S2NN) and its smoothed result (S2NNS); Column 9: laboratory measured, interpreted permeability (PERM and PermNN) and its smoothed result (PermNNS).

Table 4. Average and maximum neural network interpreted TOC content (wt %) and S2 (mg HC/g rock) of claystone (TOCsh, TOCshmax, S2sh and S2shmax) in the Middle Interval in Barnicarndy 1

Interval	TOCsh	TOCshmax	S2sh	S2shmax
M_6	0.228	0.586	0.073	0.410
M_5	0.208	0.656	0.066	0.381
M_4	0.184	0.553	0.031	0.453
M_3	0.057	0.272	0.014	0.087
M_2	0.179	0.524	0.105	0.460
M_1	0.044	0.160	0.014	0.140
Middle Interval	0.167	0.656	0.046	0.460

Table 5. Correlation coefficients (R) between the neural network estimated and laboratory measured permeability in Barnicarndy 1

Interval	Correlation coefficient (R)
Upper Sandstone	0.9667
Middle Interval	0.7473
Lower Sandstone	0.8256
All	0.9287

Table 6. Geometrical mean and maximum permeability (mD) of sandstone of the three major intervals and claystone in the Middle Interval

Lithofacies	Interval	Geometric mean	Maximum
Sandstone	Upper Sandstone	457.40	3655.8
	Middle Interval	0.004	34.39
	Lower Sandstone	0.037	630.09
Claystone	M_6	0.122	32.288
	M_5	0.005	0.339
	M_4	0.002	0.236
	M_3	0.002	0.041
	M_2	0.004	0.821
	M_1	0.002	0.222
	Middle Interval	0.006	32.288

density (RHOB, g/cm^3), compressional slowness (DT, µs/ft), limestone neutron porosity (NPHI, fraction) and deep resistivity (RDEEP, Ω m). The outputs of neural network included the weight percentages of various mineral compositions. In total, 99 training patterns were constructed for neural network learning. For the purpose of validation, 91 testing results were used for training, while 10 testing results were used as a validation set.

Fig. 7 presents the laboratory measured, neural network estimated and smoothed interpretations for the simplified mineral assemblage (Columns 5–6) and for detailed mineral assemblage (Columns 7–8) in Barnicarndy 1. Compared to the vertical distribution patterns of laboratory testing results, the neural network estimated mineral compositions have learned effectively the vertical distribution patterns inside the laboratory measurements, well logs and lithological sequences. Neural network interpretation results present continuous information on the variations of lithofacies and mineral compositions.

Table 7 lists the averages of the neural network interpreted mineral compositions and assemblages from various intervals in Barnicarndy 1.

Table 8 provides the averages of the interpreted mineral compositions and geomechanical interpretations of the claystone from the entire Middle Interval in Barnicarndy 1. Table 9 lists some correlation coefficients (R) between TOC content of claystone and the petrophysical and geomechanical properties in the entire Middle Interval in Barnicarndy 1. The integrated interpretations on claystones in the Middle Interval are summarised in the following:

1) The high values of TOC and S2 appear in M_4, M_5 and M_6 zones where the claystone mainly contains a certain amount of carbonate minerals (calcareous or dolomitic claystone) (Tables 4 and 8). TOC content has positive correlation with porosity, permeability and carbonate contents (Tables 2, 4, 6 and 9).
2) Young's modulus and Poisson's ratio have good correlations with the contents of key minerals, including quartz, carbonates and TotalClay (Table 8). The evaluation on elastic properties and mineral assemblages provides inputs for further rock brittleness analysis (Jarvie *et al.* 2007; Rickman 2008; Gray *et al.* 2012).
3) TOC content seems to be positively correlated with Poisson's ratio and negatively correlated to Young's modulus in claystone in the Middle Interval (Tables 8 and 9).

Thermal maturity and hydrocarbon generation

In the absence of vitrinite in Ordovician samples, 11 samples from the depth range of 1354.8–2244.08 mRT were examined to obtain graptolite reflectance (Ranasinghe and Crosdale 2020). The mean maximum graptolite reflectance ranges from 0.83% to 2%, and was converted to vitrinite reflectance using the model proposed in Luo *et al.* (2020) as:

$$\mathrm{EqVRo} = 0.515 \times \mathrm{GRomax} + 0.506 \tag{2}$$

where GRomax is the mean of the maximum graptolite reflectance (%) and EqVRo is the calculated equivalent vitrinite reflectance (%). The calculated equivalent vitrinite reflectance (EqVRo, %) ranges from 0.93% to 1.54%.

The Mesozoic section has either been eroded or not deposited within the Barnicarndy Graben (Whitaker *et al.* 2010; Alavi 2013). 1D petroleum systems modelling at Barnicarndy 1 possibly indicates that up to 3000 m of uplift and erosion occurred in association with the late Triassic to early Jurassic Fitzroy Transpression (MacFarlane *et al.* 2021), which may account for an inconsistency of the calculated vitrinite reflectance with the present-day temperature derived from geothermal gradient and surface temperature (Walker Petrophysics Pty Ltd 2020). Burial prior to the uplifting event pushed the Middle

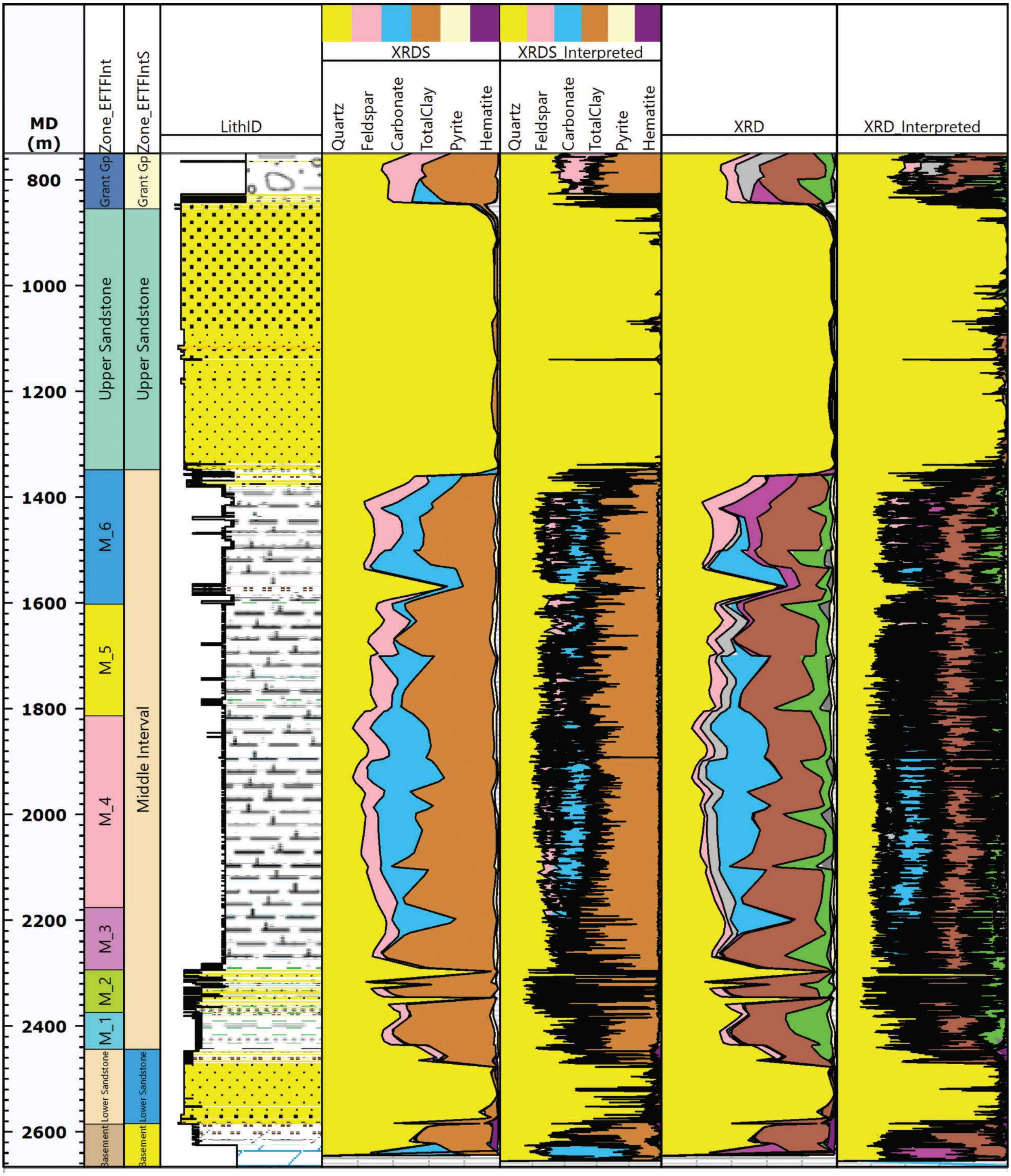

Fig. 7. Mineral composition interpretations through neural network learning. Neural network interpretation results of TOC content, S2 and permeability. Column 1: measured depth (MD); Columns 2–3: two orders of zones (Zone_EFTFInt and Zone_EFTFIntS); Column 4: lithological descriptions of cores (LithID, same legend as in Fig. 2); Column 5: laboratory measured simplified mineral assemblage (XRDS); Column 6: neural network interpreted simplified mineral assemblage (XRDS_Interpreted); Column 7: laboratory measured mineral assemblage (XRD, same legend as in Fig. 2); Column 8: neural network interpreted mineral assemblage (XRD_Interpreted).

Table 7. Averages of the interpreted mineral compositions (wt %) in Barnicarndy 1

Mineral	Upper Sandstone	M_6	M_5	M_4	M_3	M_2	M_1	Lower Sandstone
Quartz	97.47	38.15	29.29	25.67	30.89	47.87	46.37	88.15
K-feldspar	0.06	7.44	5.03	2.10	2.06	3.63	4.84	1.58
Plagioclase	0.05	2.67	8.36	7.01	2.55	0.52	1.41	0.28
Calcite	0	5.24	7.93	21.01	10.73	2.78	1.10	0.24
Dolomite	0	9.24	1.66	1.42	7.66	0.59	0.26	0.03
Mica	1.36	25.66	35.49	30.53	26.38	30.07	29.72	7.34
Chlorite	0.76	8.78	9.92	9.19	15.62	13.26	13.87	1.27
Kaolinite	0.28	1.05	0.91	1.84	2.85	0.15	0.31	0.03
Pyrite	0.01	1.75	1.39	1.22	1.40	0.81	1.48	0.06
Hematite	0.04	0.001	0.000003	0.000018	0.001	0.08	0.34	1.71

Table 8. Averages of interpreted mineral compositions and geomechanical properties of claystone for the entire Middle Interval

Parameter	M_6	M_5	M_4	M_3	M_2	M_1
Quartz (wt%)	34.20	29.29	25.62	30.89	32.31	46.37
Carbonate (wt%)	18.77	10.79	19.91	5.72	0.90	0.79
TotalClay (wt%)	35.25	46.17	42.52	50.29	45.78	42.04
YME_STA (GPa)	14.21	6.77	9.35	13.10	18.90	15.93
PR_STA (fraction)	0.142	0.164	0.160	0.152	0.136	0.136

Table 9. Correlation coefficients (R) between the TOC content of claystone and petrophysical and geomechanical properties in the Middle Interval in Barnicarndy 1

Parameter	PHIE_ND	Carbonate	YME_STA	PR_STA	logK[A]
TOC	0.4292	0.3632	–0.2430	0.1109	0.3123

[A]Logarithmic permeability.

Interval and Lower Sandstone into the oil-wet gas window (Tissot and Welte 1984; Ghori 2013; MacFarlane *et al.* 2021).

Fluid inclusions are small volumes of palaeo-fluids trapped in minerals, which provide information about geological processes (Figs 2 and 4). The inclusions can include trapped gases, liquids or multi-phase (Randive *et al.* 2014). FIS results over the depths of interest are summarised by FIT (2020) as follows:

- Mostly dry gas responses were obtained over the depth range of 827–1381 mRT with a single wet gas spectrum at 1111.1 mRT. Trace liquid/range alkanes co-vary with methane for the most part, suggesting natural hydrocarbons in the system. Sulfur species are sporadically present.
- In thin sections, rare white-fluorescent, upper-gravity petroleum inclusions were found at 1069.8 mRT (Fig. 8). Rare mixed (oil and brine) petroleum inclusions were noted at 910.9 mRT, 1111.1 mRT (Fig. 8) and 1179.6 mRT. Rare yellow-fluorescent, moderate-gravity petroleum inclusions were recorded at 1111.1 mRT. Low inclusion abundance suggests petroleum migration through the Upper Sandstone.
- Appreciable amount of immature oil-prone kerogen was found at 1354.9 mRT.
- The depth range of 1411.3–2679.1 mRT exhibits mostly sub-anomalous FIS responses, with dry gas spectra at 2312.1 mRT, 2331.8 mRT, 2447.4 mRT, 2478–2530.1 mRT and 2550.3–2580.3 mRT. The highest methane and liquid hydrocarbon responses are recorded at 2550.3–2580.3 mRT. Anomalous benzene is recorded at 2180.1 mRT, 2550.3 mRT, 2560.7 mRT, and anomalous acetic acid is noted at 2550.3 mRT. Sulfur species, such as hydrogen sulfide (H_2S), are notable at 2447.4 mRT and 2550.3–2580.3 mRT, suggesting potential for water-bearing porous reservoir rocks.

Considering the laboratory measured and interpreted TOC content, thermal maturity and fluid inclusion analysis results, the organic matter in the Middle Interval and Lower Sandstone has entered the oil-wet gas window. Hydrocarbon inclusions indicate that hydrocarbon generation and migration have occurred elsewhere in the depocentre of Barnicarndy Graben, although TOC content is low at Barnicarndy 1.

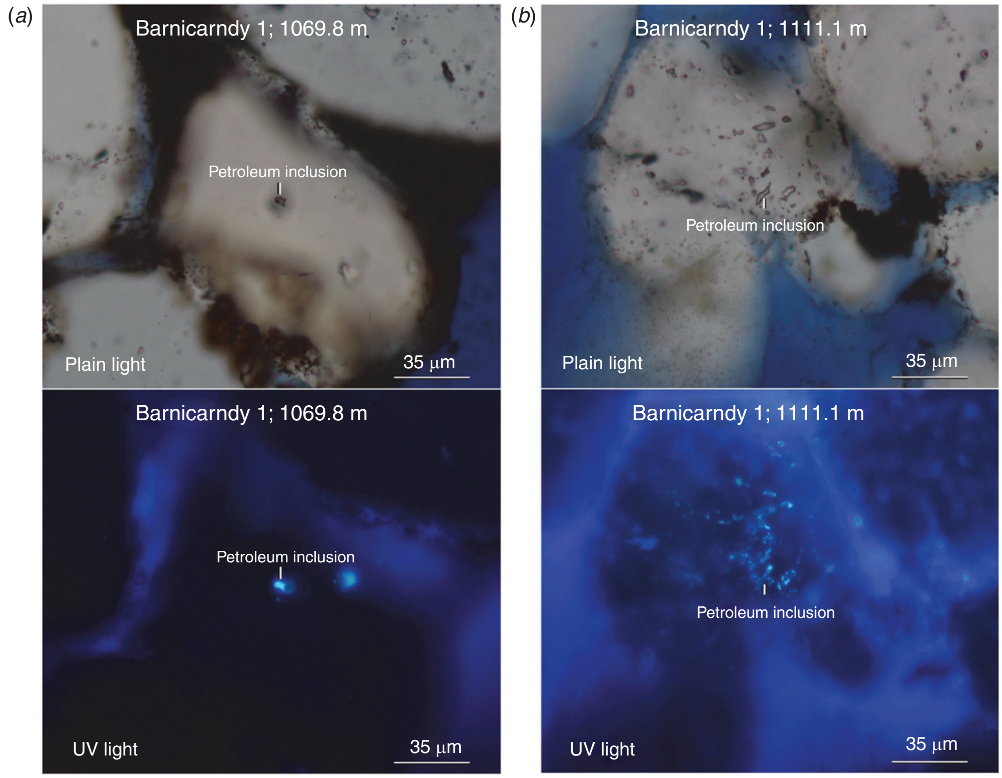

Fig. 8. Photomicrographs of petroleum inclusions found at (*a*) 1069.8 mRT and (*b*) 1111.1 mRT in Barnicarndy 1 (FIT 2020).

Conclusions

Conventional methods and ANN modelling have been used to interpret the petrophysical, geomechanical and organic geochemical properties, and mineral compositions from well logs in the pre-Carboniferous succession in Barnicarndy 1. The main results and conclusions of this study are listed as follows:

- The depth range of 855–2585 mRT was divided into three major intervals as: Upper Sandstone (855–1348.1 mRT), Middle Interval (1348.1–2443.4 mRT) and Lower Sandstone (2443.4–2585 mRT), considering lithology, well logs, chemostratigraphy, XRD, fluid inclusion tests, HyLogger data, etc. The Middle Interval comprises claystone with minor siltstone/sandstone and is divided into six internal zones based on lithofacies variations.
- Average sandstone porosities of the Upper Sandstone and Lower Sandstone are 17.9% and 6.75%. Average reservoir porosities of the Upper Sandstone and Lower Sandstone are 18% and 12.7%, and average claystone porosity is 4.17% in the Middle Interval. The ratios of reservoir/gross thickness in the Upper Sandstone and Lower Sandstone are 0.991 and 0.243.
- The geometric means of reservoir permeability of the Upper Sandstone and Lower Sandstone are 464.5 mD and 10 mD. The geometric mean of claystone permeability in the Middle Interval is 0.006 mD.
- Average TOC content and S2 of claystone in the Middle Interval are 0.17 wt% and 0.047 mg HC/g Rock. TOC content has a positive correlation with porosity, permeability and carbonate content in the Middle Interval.
- Average Poisson's ratio and Young's modulus of claystone in the Middle Interval are 0.154 and 9.81 GPa. Young's modulus and Poisson's ratio are well correlated with the contents of key minerals, including quartz, carbonates and TotalClay. The evaluations on elastic properties and mineral assemblages provide inputs for further rock brittleness analysis.
- Hydrocarbon generation and migration have occurred elsewhere in the Barnicarndy Graben even though TOC content is low at Barnicarndy 1.

Conflicts of interest

The authors declare no conflicts of interest.

Declaration of funding

As part of Geoscience Australia's Exploring for the Future program, this study was conducted in collaboration with and co-funded by the Government of Western Australia's Exploration Incentive Scheme.

Acknowledgements

We thank Steve Abbott and Duy Nguyen for internal peer reviews at Geoscience Australia. This paper is published with the permission of the CEO, Geoscience Australia. L. Normore and P. Haines publish with the permission of the Executive Director of the Geological Survey of Western Australia. Based on consultation with the Western Desert Lands Aboriginal Corporation (WDLAC) on the cultural significance of the name, Waukarlycarly, it has been agreed to change the name of the well to Barnicarndy 1 and the

tectonic subdivision to Barnicarndy Graben. This and all future publications will now refer to the Barnicarndy 1 stratigraphic drillhole (previously Waukarlycarly 1) and the Barnicarndy Graben (previously Waukarlycarly Embayment).

References

Alavi, S. N. (2013). Structure, stratigraphy, and petroleum prospectivity of the Waukarlycarly Embayment, Canning Basin, Western Australia. Geological Survey of Western Australia, Record 2013/10, 32p.

Backhouse, J. (2020). Waukarlycarly 1: Palynology of 7 samples. Backhouse Biostrat P/L. Report prepared for Department of Mines, Industry Regulation and Safety. Available at https://wapims.dmp.wa.gov.au/WAPIMS/Search/Wells [Verified 19 January 2021].

Bagas, L., Anderson, J. A. C., and Bierlein, F. P. (2009). Palaeoproterozoic evolution of the Killi Killi Formation and orogenic gold mineralization in Granite-Tanami Orogen, Western Australia. *Ore Geology Reviews* **35**, 47–67. doi:10.1016/j.oregeorev.2008.09.001

Behar, F., Beaumont, D. B., and Penteado, H. L. (2001). Rock-Eval 6 technology: performances and developments. *Oil & Gas Science and Technology – Rev. IFP* **56**(2), 111–134. doi:10.2516/ogst:2001013

Carr, L. K., Edwards, D. S., Southby, C., Henson, P., Haines, P. W., Normore, L., Zhan, A., Brooks, D., MacFarlane, S., Boreham, C. J., Grosjean, E., Mory, A. J., Wang, L., and Gunning, M-E. (2020). Kidson Sub-basin seismic survey and Waukarlycarly 1 stratigraphic well: an acquisition program for evaluating Canning Basin petroleum systems. In 'Exploring for the Future: Extended Abstracts'. (Eds K. Czarnota, I. Roach, S. Abbott, M. Haynes, N. Kositcin, A. Ray and E. Slatter.) pp. 1–4. (Geoscience Australia, Canberra). doi:10.11636/134073

Core Lab (2020*a*). Routine core analysis report, Waukarlycarly 1, Western Australia. Report prepared for Department of Mines, Industry Regulation and Safety. Core Laboratories Australia Pty Ltd. Available at https://wapims.dmp.wa.gov.au/WAPIMS/Search/Wells [Verified 19 January 2021].

Core Lab (2020*b*). Petrographic analysis of rotary sidewall cores, Waukarlycarly 1, Canning Basin, Australia. Available at https://wapims.dmp.wa.gov.au/WAPIMS/Search/Wells [Verified 19 January 2021].

Edwards, D. S., Gilmore, S., Wang, L., and Grosjean, E. (2021). Inorganic geochemical results for Barnicarndy 1, Canning Basin, Western Australia. Geoscience Australia Record (eCat 144558). In preparation.

FIT (2020). A stratigraphic reconstruction of bulk volatile chemistry from fluid inclusions in Waukarlycarly 1. Prepared by FIT for Geoscience Australia. Available at https://wapims.dmp.wa.gov.au/WAPIMS/Search/Wells [Verified 19 January 2021].

Forbes, A., Sullivan, N., Edwards, D. S., and Grosjean, E. (2020). Chemostratigraphy of Waukarlycarly-1, Canning Basin, Western Australia. Report CAu50017. Chemostrat Australia Pty, 2020. Available at https://wapims.dmp.wa.gov.au/WAPIMS/Search/Wells [Verified 19 January 2021].

Geological Survey of Western Australia (GSWA) (2020*a*). HyLogger record 2020/6, Appendix I HyLogger-3 core summary HyLogger Rec 2020_6, W006030 A1.zip. Available at https://wapims.dmp.wa.gov.au/WAPIMS/Search/Wells [Verified 19 January 2021].

Geological Survey of Western Australia (GSWA) (2020*b*). HyLogger record 2020/7, Appendix H HyLogger-3 ditch cuttings summary HyLogger Rec 2020_7, W006030 A1.zip. Available at https://wapims.dmp.wa.gov.au/WAPIMS/Search/Wells [Verified 19 January 2021].

Geological Survey of Western Australia (GSWA) (2020*c*). Barnicarndy 1 well completion report. Available at https://wapims.dmp.wa.gov.au/WAPIMS/Search/Wells [Verified 19 January 2021].

Ghori, K. A. R. (2013). Emerging unconventional shale plays in Western Australia. *The APPEA Journal* **53**, 313–336. doi:10.1071/AJ12027

Gray, D., Anderson, P., Logel, J., Delbecq, F., Schmidt, D., and Schmid, R. (2012). Estimation of stress and geomechanical properties using 3D seismic data. *First Break* **30**, 59–68. doi:10.3997/1365-2397.2011042

Grosjean, E., Edwards, D. S., Boreham, C. J., Hong, Z., Chen, J., Jinadasa, N., and Buckler, T. (2020). Rock-Eval pyrolysis data from Waukarlycarly 1, Canning Basin, Australia. Destructive Analysis Report 2020-003. Available at https://wapims.dmp.wa.gov.au/WAPIMS/Search/Wells [Verified 19 January 2021].

Hect-Nielsen, R. (1990). 'Neurocomputing.' (Addison-Wesley: Menlo Park, CA, USA.)

Herron, S. L. (1991). In situ evaluation of potential source rocks by wireline logs. In 'Source and Migration Processes and Evaluation Techniques. Treatise of Petroleum Geology. Handbook of Petroleum Geology'. (Eds N. H. Foster and E. A. Beaumont.) pp. 127–134. (American Association of Petroleum Geologists: USA.)

Hopfield, J. J. (1985). 'Neural' computation of decisions in optimization problem. *Biological Cybernetics* **52**, 141–152.

Huang, Y., Gedeon, T. D., and Wong, P. M. (2001). An integrated neural-fuzzy-genetic-algorithm using hyper-surface membership functions to predict permeability in petroleum reservoirs. *Engineering Applications of Artificial Intelligence* **14**(2001), 15–21. doi:10.1016/S0952-1976(00)00048-8

Jarrett, A. J. M., Bailey, A. H. E., Dewhurst, D. N., Esteban, L., Kager, S., and Monmusson, L. (2020). Exploring for the Future - Waukarlycarly 1 petrophysical testing program data release, Canning Basin, Australia. Record 2020/28. Geoscience Australia, Canberra. doi:10.11636/record.2020.028

Jarvie, D. M., Hill, R. J., Ruble, T. E., and Pollastro, R. M. (2007). Unconventional shale-gas systems: the Mississippian Barnett Shale of north-central Texas as one model for thermogenic shale-gas assessment. *AAPG Bulletin* **91**(4), 475–499. doi:10.1306/12190606068

Kalogirou, S. A. (2000). Applications of artificial neural-networks for energy systems. *Applied Energy* **67**(1–2), 17–35. doi:10.1016/S0306-2619(00)00005-2

Kennard, J. M., Jackson, M. J., Romine, K. K., Shaw, R. D., and Southgate, P. N. (1994). Depositional sequences and associated petroleum systems of the Canning Basin, WA. In 'The Sedimentary Basins of Western Australia.' (Eds P. G. Purcell and R. R. Purcell.) pp. 657–676. (Proceedings of the Petroleum Exploration Society of Australia Symposium: Perth, WA, 1994.)

Luo, Q., Fariborz, G., Zhong, N., Wang, Y., Nansheng Qiu, N., Skovsted, C. B., Suchý, V., Schovsbo, N. H., Morga, R., Xu, Y., Hao, J., Liu, A., Wu, J., Cao, W., Min, X., and Wu, J. (2020). Graptolites as fossil geothermometers and source material of hydrocarbons: an overview of four decades of progress. *Journal of Earth-Science Reviews* **200**(2020). doi:10.1016/j.earscirev.2019.103000

MacFarlane, S. K., Palu, T. J., Edwards, D. S., Boreham, C. J., Wang, L., Grosjean, E., Carr, L. K., and Henson, P. (2021). Canning Basin: Petroleum systems modelling and associated data analysis in the Kidson and Willara sub-basins and the Barnicarndy Graben. Geoscience Australia Record (eCat144508). In preparation.

Normore, L. S., and Rapaic, M. (2020). Barnicarndy 1 basic data: well completion report. Geological Survey of Western Australia. Report 206, 2020. Available at https://wapims.dmp.wa.gov.au/WAPIMS/Search/Wells [Verified 19 January 2021].

Normore, L. S., and Zhan, Y. (2020). Exploring the southwest Canning Basin: GSWA Waukarlycarly 1 and the Kidson Sub-basin seismic survey. GSWA 2020 extended abstract, Perth. Available at https://dmpbookshop.eruditetechnologies.com.au//product/exploring-the-southwest-canning-basin-gswa-waukarlycarly-1-and-the-kidson-sub-basin-seismic-survey.do [Verified 19 January 2021].

Normore, L., Haines, P. W., Carr, L. K., Henson, P., Zhan, Y., Wingate, M. T. D., Zhen, Y. Y., Lu, Y., Martin, S., Kelsey, D., Allen, H., and Fielding, I. (2021). Barnicarndy Graben, southern Canning Basin: stratigraphy defined by the Barnicarndy 1 stratigraphic well. *The APPEA Journal* **61**, 224–235. doi:10.1071/AJ20160

Ouadfeul, S. A., and Aliouane, L. (2015). Total organic carbon prediction in shale gas reservoirs from well logs data using the multilayer perceptron neural network with Levenberg Marquardt training algorithm: application to Barnett Shale. *Arabian Journal for Science and Engineering* **40**(11), 3345–3349. doi:10.1007/s13369-015-1685-y

Passey, Q. R., Creaney, S., Kulla, J. B., Moretti, F. J., and Stroud, J. D. (1990). A practical model for organic richness from porosity and resistivity logs. *AAPG Bulletin* **74**(12), 1777–1794.

Passey, Q. R., Bohacs, K. M., Esch, W. L., Klimentidis, R., and Sinha, S. (2010). From oil-prone source rock to gas-producing shale reservoir – geologic and petrophysical characterization of unconventional shale-gas reservoirs. SPE 131350, CPS/SPE International Oil & Gas Conference and Exhibition, Beijing, China, 8–10 June 2010. doi:10.2118/131350-MS

Ranasinghe, S.P., and Crosdale, P. J. (2020). Report on source rock type, maturation levels and hydrocarbon potential of a suite of samples from Waukarlycarly-1 in the Canning Basin, Western Australia. Report prepared by Energy Resources Consulting Pty Ltd for Geoscience Australia, Canberra. Available at https://wapims.dmp.wa.gov.au/WAPIMS/Search/Wells [Verified 19 January 2021].

Randive, K. R., Hari, K. R., Dora, M. L., Malpe, D. B., and Bhondwe, A. A. (2014). Study of fluid inclusions: methods, techniques and applications. Gondwana *Geological Magazine* **29**(1 and 2), 19–28.

Rickman, R. (2008). A practical use of shale petrophysics for stimulation design optimization: all shale plays are not clones of the Barnett shale. SPE Annual Technical Conference and Exhibition, 21–24 September 2008, Denver, Colorado, USA, SPE 115258. doi:10.2118/115258-MS

Schlumberger (1991). Log Interpretation Principles/Applications. (Schlumberger Educational Services: Houston, Texas, USA.)

Schmoker, J. W. (1981). Determination of organic-matter content of Appalachian Devonian shales from gamma-ray logs. *AAPG Bulletin* **65**, 1285–1298.

Schmoker, J. W., and Hester, T. C. (1983). Organic carbon in Bakken Formation, United States portion of Williston Basin. *AAPG Bulletin* **67**, 2165–2174.

Tissot, B. P., and Welte, D. H. (1984). 'Petroleum Formation and Occurrence'. 2nd edn. (Springer-Verlag: Berlin.)

Walker Petrophysics Pty Ltd (2020). Petrophysical evaluation, Waukarlycarly 1. Walker Petrophysics Pty Ltd, WAPIMS. Available at https://wapims.dmp.wa.gov.au/WAPIMS/Search/Wells [Verified 19 January 2021].

Wang, L., Edwards, D. S., Bailey, A., Carr, L. K., Boreham, C. J., Grosjean, E., Anderson, J., Jarrett, A. J. M., McFarlane, S., Southby, C., Carson, C., Khider, K., Palu, T., and Henson, P. (2021). Well Log Data Analysis and Interpretation on the Pre-Carboniferous Succession in Waukarlycarly 1, Canning Basin, Western Australia. (Record 2021/03, Geoscience Australia.) http://dx.doi.org/10.11636/Record.2021.003

Weatherford (2007). Log Interpretation Charts, Compact™ Tools Series. Document 4060.01. (Weatherford: Houston, Texas, USA.)

Whitaker, A. J., Roach, I. C., Liu, S. F., and Wilford, J. R. (2010). Geology. In 'Geological and Energy Implications of the Paterson Airborne Electromagnetic (AEM) Survey, Western Australia'. (Eds I. C. Roach), pp. 49–86. (Record 2010/12, Geoscience Australia.)

Wong, P. M., Jian, F. X., and Taggart, I. J. (1995). A critical comparison of neural networks and discriminant analysis in lithofacies, porosity and permeability predictions. *Journal of Petroleum Geology* **18**(2), 191–206. doi:10.1111/j.1747-5457.1995.tb00897.x

Yan, W., Wang, J., Liu, S., Wang, K., and Zhou, Y. (2014). Logging identification for the Longmaxi mud shale reservoir in the Jiaoshiba area, Sichuan Basin. *Natural Gas Industry* **34**(6), 30–36. doi:10.1016/j.ngib.2014.11.016

Zhan, Y., and Mory, A. J. (2013). Structural interpretation of the Northern Canning Basin, Western Australia. West Australian Basins Symposium 2013, Perth WA, August 2013. PDF 978-1-74168-440-7. Available at http://www.academia.edu/17437490/Structural_Interpretation_of_the_Northern_Canning_Basin_Western_Australia [Verified 19 January 2021].

The authors

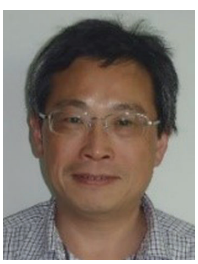

Liuqi Wang is a Well Analyst at Geoscience Australia, working in the Minerals, Energy and Groundwater Division. He received his PhD in Petroleum Engineering and worked as a Research Fellow at the University of New South Wales before joining Geoscience Australia. His research interests include petrophysics, static and dynamic reservoir modelling, applied statistics and artificial intelligence. He is a member of PESA and EAGE.

Dianne S. Edwards is a Principal Petroleum Geochemist at Geoscience Australia, working in the Minerals, Energy and Groundwater Division. Her scientific focus is on defining the petroleum systems of Australia's petroliferous basins, including both conventional and unconventional play types. She is involved in building database systems to release petroleum geochemical data via the portal https://portal.ga.gov.au. Dianne received her BSc (Hons) degree in Geology and MSc in Organic Petrology and Organic Geochemistry from the University of Newcastle-upon-Tyne (UK). She was awarded her PhD from the University of Adelaide in 1996. In 2018, she received the Australian Organic Geochemistry Conference Medal for lifetime achievement in the field of Organic Geochemistry. Dianne is a member of PESA.

Adam H.E. Bailey is a Petroleum Geoscientist at Geoscience Australia, with expertise in petroleum geomechanics, structural geology and basin analysis. He graduated with a BSc (Hons) in 2012 and a PhD in 2016 from the Australian School of Petroleum at the University of Adelaide. Working with the Onshore Energy Systems team at Geoscience Australia, Adam is currently working on the flagship Exploring for the Future Program in Northern Australia and is the geology discipline lead for the Geological and Bioregional Assessment Programme.

Lidena K. Carr is a Geoscientist for the Onshore Energy Systems program within the Resources Division at Geoscience Australia. She graduated from the Australian National University (ANU), majoring in Geology and Human Ecology, with a BA/BSc (Hons) in 2004 and began working as a technical officer at the Research School of Earth Sciences (ANU). In 2007, she joined Geoscience Australia with the then ACRES (satellite imagery). In 2009, she moved to the then Onshore Energy and Mineral Division to work as a Seismic Interpreter and Basin Analyst. Currently, she is the acting Director of the Onshore Energy Systems directorate working on the Exploring for the Future program. She is member of PESA and GSA.

Christopher J. Boreham is a Principal Petroleum Geochemist at Geoscience Australia, working in the Minerals, Energy and Groundwater Division. He obtained his BSc (Hons) in Chemistry from the University of Queensland and was awarded a PhD in Chemistry at ANU. He has worked at Geoscience Australia for four decades. Chris has a wide experience in the application of organic geochemistry to the evolution of oil and gas in Australian sedimentary basins. He has recently extended these geochemical studies to unconventional petroleum (coal seam methane, shale gas and oil), helium, hydrogen and abiogenic hydrocarbons, as well as being involved in CO2CRC's studies on the injection of CO_2 into a depleted natural gas field and a saline aquifer. In 2010, he received the Australian Organic Geochemistry Conference Medal for lifetime achievement in the field of Organic Geochemistry. Chris is a member of PESA.

Emmanuelle Grosjean is an Organic Geochemist at Geoscience Australia, working in the Minerals, Energy and Groundwater Division. Emmanuelle applies organic geochemistry to assess the hydrocarbon prospectivity of Australia's offshore and onshore sedimentary basins. Emmanuelle holds a PhD in Organic Chemistry from the University of Strasbourg, France. Before joining Geoscience Australia in 2005, she worked on the Precambrian petroleum systems of the South Oman Salt Basin as a Post-doctoral Associate at the Massachusetts Institute of Technology.

For the past eight years Leon Normore has been a Senior Geologist in the Geological Survey and Resource Strategy Division, Department of Mines, Industry Regulation and Safety at the Geological Survey of Western Australia, focused primarily on the Canning Basin of Western Australia. Leon's previous work includes petroleum and mineral exploration in Canada and the United States, as well as regional mapping with the Geological Survey of Newfoundland and Labrador.

Jade Anderson works as a Geoscientist in basin systems at Geoscience Australia. She completed a PhD at the University of Adelaide in 2015 in the areas of metamorphic geology, geochronology and Proterozoic Australia tectonics.

Amber Jarrett is a Geochemist in the Minerals, Energy and Groundwater Division, Geoscience Australia. Her research interests include basin hosted resource potential, organic-inorganic geochemistry, isotopes, Proterozoic biomarkers and early life. Amber graduated with BSc (Hons), majoring in both Geology and Biology 2008, and a PhD in 2014 from ANU. Amber is also a key researcher in the MinExCRC.

Susannah K. MacFarlane is a Petroleum Geoscientist at Geoscience Australia, working in the Onshore Energy Systems team. Susannah did her undergraduate degree and PhD at the University College London, graduating in 2008. She subsequently spent several years working for industry in the UK and Australia before joining Geoscience Australia in 2016. Her current research interests are basin analysis and petroleum systems modelling.

Chris Southby is a Geoscientist in the Geoscience Australia Resources Division, Energy Systems Branch. He completed his Honours at ANU in 2004 on palaeo-climate geochemistry of corals from Papua New Guinea. Since joining Geoscience Australia in 2008, he has contributed to a number of projects, including the National Carbon Mapping and Infrastructure Plan, the Vlaming Sub-basin CO2 Storage Assessment and the Houtman Sub-basin Prospectivity Project. He is now part of the Onshore Energy Systems team at Geoscience Australia, currently working under the Exploring for the Future program initiative.

Chris Carson has worked in Antarctica, Canadian Arctic, Alaska, New Caledonia and northern and central Australia, specialising in metamorphic petrology, geochronology and structural geology. Joining Geoscience Australia in 2006, he dabbled in SHRIMP geochronology and, in 2017, joined the Onshore Energy program, working in the South Nicholson region of the NT.

Kamal Khider is a Senior Geoscientist in Geoscience Australia's Resources Division, Energy Systems Branch. He has a BSc, MSc and PhD (Stratigraphy and Sedimentology) and a PhD in Applied Geochemistry. Kamal has long standing academic and consultative experience in geosciences, working in many academic and industrial geological organisations in Australia, the Middle East and North Africa. He worked on the regional geological appraisal of the Eocene–Oligocene–Miocene boundaries IGCP 174, regional geochemical assessment of the Cobar-Girilambone region in NSW and the Queensland Carbon Dioxide Geological Storage Atlas. Since 2007, he has worked on several of Geoscience Australia's petroleum and carbon capture and storage projects. Kamal is a member of AAPG, GSA and SEPM.

Paul A. Henson graduated from the University of Tasmania and is currently the Director of the Onshore Energy Systems Section at Geoscience Australia. He has extensive experience in the minerals sector, working on mineral systems in Proterozoic and Archaean terranes. Since 2010, he led the Australian Governments' onshore carbon storage program, undertaking deep onshore drilling and seismic acquisition programs in collaboration with the states and industry. In addition, he now manages the Exploring for the Future - Energy Program, leading a team of researchers to acquire new pre-competitive geoscientific data to improve our understanding of the oil and gas potential of Australian onshore basins.

Peter Haines holds Honours and PhD degrees in Geology from the University of Adelaide. He has previously held positions at the Northern Territory Geological Survey and Universities of South Australia, Adelaide and Tasmania. He joined the Geological Survey of Western Australia in 2003, currently holding title of Basins Custodian within the Energy Geoscience and Carbon Strategy Branch. He is a member of PESA and GSA.

Mike Walker is currently the Principal Petrophysicist for Walker Petrophysics Pty Ltd, Mike has 39 years of oil industry experience with major operators and small companies and a major service company. Prior to founding Walker Petrophysics in 2004, Mike was Staff (Region) Petrophysicist for Baker Atlas Geoscience, the geological consulting and interpretation arm of Baker Hughes for six years, which involved him working as a consultant for external clients and as well as a mentor and advisor inside the company. Before that, he worked as Senior Petrophysicist with Woodside and BHP petroleum and Petroleum Geologist with CSR Petroleum. Mike obtained his BSc (Hons) in Applied Geology form the University of New South Wales in 1981. He also has undertaken local and remote mentoring projects with junior professional staff and technical assistants and has also provided on-the-job training for local professionals in China, Indonesia, Malaysia, Bangladesh and Vietnam.